

Efficient Iris Recognition Scheme Based on Difference of Filters

G.S.El-taweel* A.K.Helmy**

* Computer Science, Faculty of Computers and Informatics, Suez Canal University

** National Authority of Remote Sensing and Space Sciences

23 titio st., el Nozha el-gidida, Cairo, Egypt

ghada_el11@hotmail.com ; akhelmy@narss.sci.eg

Abstract: - With a growing emphasis on human identification, iris recognition has recently received increasing attention. In this paper, an efficient biometric scheme for iris recognition system with high performance is introduced. First, the irises are localized using an effective integral differential operator. Then the localized iris image is normalized to handle different size, variation in illumination and pupil dilation.

Finally, we propose a novel and efficient approach to iris feature extraction using a set of filters, called difference-of-sum filters. These filters can take advantage of a pre-computed integral image, which makes the filtering process take constant computation time no matter how big the filters are. Experimental evaluation shows that the new method has higher recognition accuracy and is faster than previous methods. The false acceptance rate was reduced by 7% in comparison with the iris code method.

Key-Words: - Biometrics, Iris normalization, Iris localization, Iris Recognition, Feature Extraction, Difference of Sum Filters.

1 Introduction

Reliable automatic recognition of persons has long been an attractive goal. As in all pattern recognition problems, the key issue is the relation between interclass and intra-class variability: objects can be reliably classified only if the variability among different instances of a given class is less than the variability between different classes. For example in face recognition, difficulties arise from the fact that the face is a changeable social organ displaying a variety of expressions, as well as being an active 3D object whose image varies with viewing angle, pose, illumination, accoutrements, and age. It has been shown that for facial images taken at least one year apart, even the best current algorithms have error rates of 43%. Against this intra-class (same face) variability, inter-class variability is limited because different faces possess the same basic set of features, in the same canonical geometry.

For all of these reasons, iris patterns become interesting as an alternative approach to reliable visual recognition of persons when imaging can be done at distances of less than a meter, and especially

when there is a need to search very large databases without incurring any false matches despite a huge number of possibilities. Although small (11 mm) and sometimes problematic to image, the iris has the great mathematical advantage that its pattern variability among different persons is enormous. In addition, as an internal (yet externally visible) organ of the eye, the iris is well protected from the environment and stable over time. As a planar object its image is relatively insensitive to angle of illumination, and changes in viewing angle cause only affine transformations; even the non-affine pattern distortion caused by pupillary dilation is readily reversible. Finally, the ease of localizing eyes in faces, and the distinctive annular shape of the iris, facilitates reliable and precise isolation of this feature and the creation of a size-invariant representation.

2. Previous Work

Daugman was the first to present a complete iris recognition system [1]. In it, the iris is localized by an integro-differential operator and unwrapped into

a rectangular image; then a set of 2D Gabor filters were applied to the unwrapped image and the quantized local phase angles were used for iris encoding. The resulting binary feature vector is called the iris code [3]. Two binary iris codes are matched using the Hamming distance. Wildes proposed another iris recognition system [4] where Laplacian of Gaussian filters were applied for iris feature extraction and the irises were matched using normalized cross-correlation. In [6], zero-crossings of the wavelet transform at various scales on a set of 1D iris rings were proposed for iris feature extraction. A 2D wavelet transform was used in [6] and quantized to form an 87-bit code. This method can not deal with the eye rotation problem, which is common in iris capture. Masek implemented an iris recognition system using a 1D log-Gabor filter [8] for binary iris code extraction. Ma *et al.* [7] used two circular symmetric filters and computed the mean and standard deviation in small blocks for iris feature extraction, with feature dimension 1,536. The authors also compared different methods for iris feature extraction, and concluded that their method outperforms many others but is not as good as Daugman's iris code. Recently, a method based on local variation analysis using a 1D wavelet transform was proposed [9]. The authors reported that their method has comparable recognition accuracy to Daugman's iris code, but only evaluated it using 200 iris images. In addition, their method used 1D processing instead of 2D. In [10], a method was proposed to characterize the local gradient direction for iris feature extraction. They claimed that their method has recognition accuracy comparable to the iris code, but it was much more complicated to compute and the extracted feature vector is 960 bytes, which is about 3 times bigger than the iris code.

Wildes' system [25] is also a patented iris recognition system. It uses the gradient-based Hough transform to decide the two circular boundaries of an iris.

Daugman's iris code method [4] is still the state-of-the-art algorithm in terms of recognition accuracy and computational complexity. Next, we develop a new method that is much simpler and faster to compute in 2D and has higher recognition accuracy than Daugman's iris code method.

3. Recognition Scheme

An iris recognition system begins with eye image capture, as shown in Figure 3.1. The system first locates the iris in the captured image. This is a very important step for iris recognition. If the iris cannot be localized correctly, the system will fail in recognizing the person. The correctly localized irises are then normalized into rectangular images called unwrapped images with a predefined size. Iris features are then extracted from the unwrapped images and used for iris matching.

3.1 Image acquisition

This step is one of the most important and deciding factors for obtaining a good result. A good and clear image eliminates the process of noise removal and also helps in avoiding errors in calculation. In this case, computational errors are avoided due to absence of reflections, and because the images have been taken from close proximity. This paper uses the image provided by CASIA [16]. These images were taken solely for the purpose of iris recognition software research and implementation. Infra-red light was used for illuminating the eye, and hence they do not involve any specular reflections. Some part of the computation which involves removal of errors due to reflections in the image were hence not implemented.

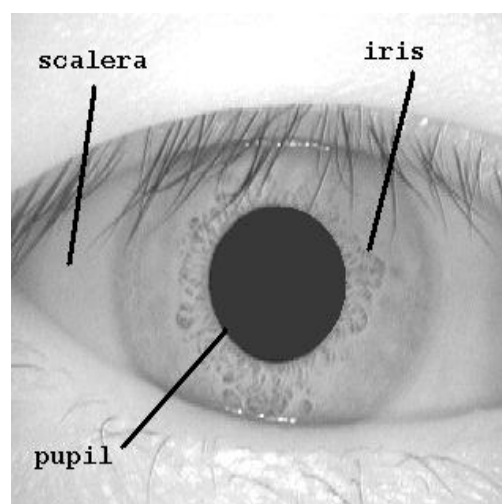


Figure1: Image of the eye

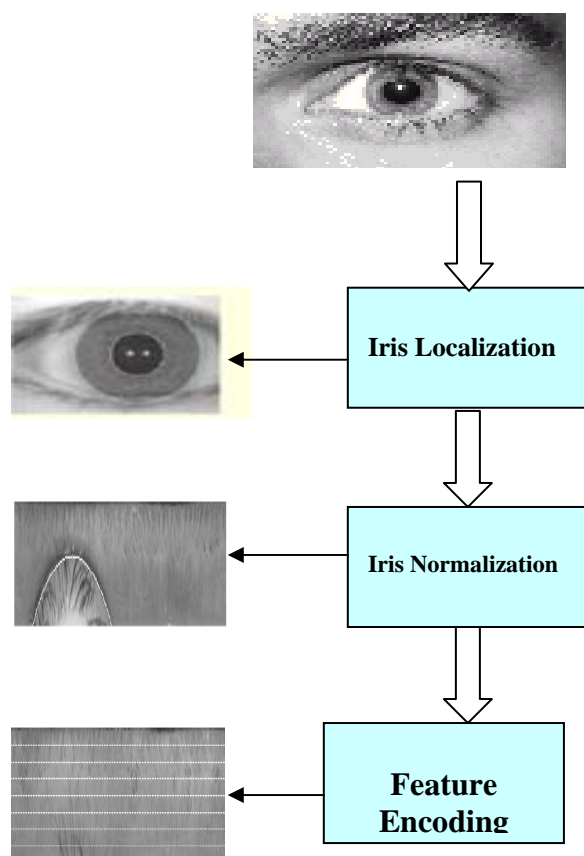


Figure2. Block diagram for proposed Scheme.

3.2 Image Pre-Processing

Due to computational ease, the image was scaled down by 60%. The image was filtered using Gaussian filter, which blurs the image and reduces effects due to noise. The degree of smoothening is decided by the standard deviation, σ and it is taken to be 2 in this case.

3.3 Iris Localization

The part of the eye carrying information is only the iris part. It lies between the sclera and the pupil. Hence the next step is separating the iris part from the eye image. The iris inner and outer boundaries are located by finding the edge image using the canny edge detector.

The Canny detector mainly involves three steps, viz. finding the gradient, non-maximum suppression and the hysteresis thresholding. As proposed by Wildes, the thresholding for the eye image is performed in a vertical direction only, so that the influence due to

the eyelids can be reduced. This reduces the pixels on the circle boundary, but with the use of Hough transform, successful localization of the boundary can be obtained even with the absence of few pixels. It is also computationally faster since the boundary pixels are lesser for calculation.

Using the gradient image [21], the peaks are localized using non-maximum suppression. It works in the following manner. For a pixel $\text{img}_{\text{grad}}(x,y)$, in the gradient image, and given the orientation $\theta(x,y)$, the edge intersects two of its 8 connected neighbors. The point at (x,y) is a maximum if its value is not smaller than the values at the two intersection points.

The next step, hysteresis thresholding, eliminates the weak edges below a low threshold, but not if they are connected to an edge above a high threshold through a chain of pixels all above the low threshold. In other words, the pixels above a threshold T_1 are separated. Then, these points are marked as edge points only if all its surrounding pixels are greater than another threshold T_2 . The threshold values were found by trial and error, and were obtained as 0.2 and 0.19. Edge detection is followed by finding the boundaries of the iris and the pupil. Daugman proposed the use of the Integro-differential operator to detect the boundaries and the radii. It is given by

$$\max_{(x_0, y_0, r)} \left| G_{\sigma}(r) * \frac{\partial}{\partial r} \int_{x_0, y_0, r} \frac{I(x, y)}{2\pi r} ds \right| \quad (1)$$

Where $I(x, y)$ is the original image. This behaves as a circular edge detector by searching the gradient image along the boundary of circles of increasing radii. From the likelihood of all circles, the maximum sum is calculated and is used to find the circle centres and radii.

The Hough transform is another way of detecting the parameters of geometric objects, and in this case, has been used to find the circles [20] in the edge image. For every edge pixel, the points on the circles surrounding it at different radii are taken, and their weights are increased if they are edge points too, and these weights are added to the accumulator array. Thus, after all radii and edge pixels have been searched, the maximum from the accumulator array is used to find the center of the circle and its radius. The Hough transform is performed for the iris outer boundary using the whole image, and then is

performed for the pupil only, instead of the whole eye, because the pupil is always inside the iris. There are a few problems with the Hough transform. Firstly, the threshold values are to be found by trial. Secondly, it is computationally intensive. This is improved by just having eight-way symmetric points on the circle for every search point and radius. The eyelashes were separated by thresholding, and those pixels were marked as noisy pixels,

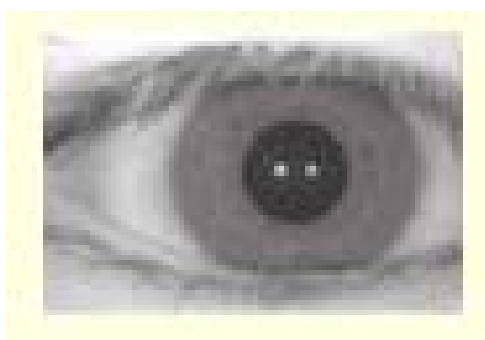
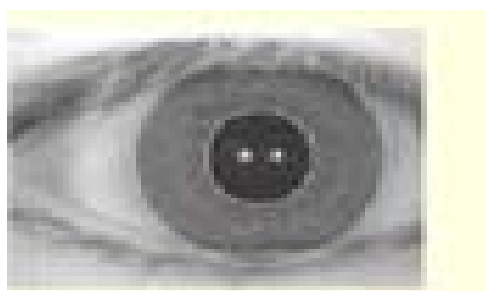


Figure2. (a) Original iris



(b) Edge Detector



(c) Iris localization

3.4 Iris Normalization

Localizing iris from an image delineates the annular portion from the rest of the image. The concept of rubber sheet modal suggested by Daugman [1] takes into consideration the possibility of pupil dilation and appearing of different size in

different images. For this purpose, the coordinate system is changed by unwrapping the iris and mapping all the points within the boundary of the iris into their polar equivalent as shown in Figure3. The mapped image has 80×360 pixels. It means that the step size is same at every angle. Therefore, if the pupil dilates the same points are picked up and mapped again which makes the mapping process stretch invariant [3]. Thus the following set of equations are used to transform the annular region of iris into polar equivalent

$$I(x(\rho, \theta), y(\rho, \theta)) \rightarrow I(\rho, \theta) \quad 2$$

with

$$x_p(\rho, \theta) = x_{p_0}(\theta) + r_p * \cos(\theta)$$

$$y_p(\rho, \theta) = y_{p_0}(\theta) + r_p * \sin(\theta)$$

$$x_i(\rho, \theta) = x_{i_0}(\theta) + r_i * \cos(\theta)$$

$$y_i(\rho, \theta) = x_{i_0}(\theta) + r_i * \sin(\theta)$$

where r_p and r_i are respectively the radius of pupil and the iris, while $(x_p(\theta), y_p(\theta))$ and $(x_i(\theta), y_i(\theta))$ are the coordinates of the pupillary and limbic boundaries in the direction θ . The value of θ belongs to $[0; 2\pi]$, ρ belongs to $[0; 1]$.

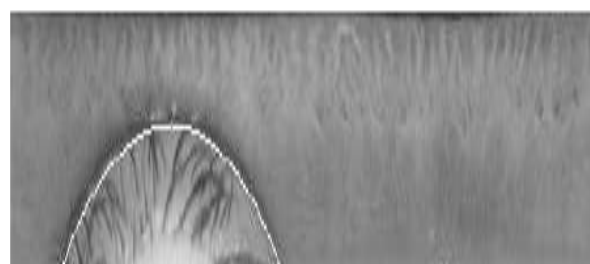


Figure3. Iris image normalization

3.5 Proposed Iris Feature Encoding

A new set of filters, called difference-of-sum filters, is introduced to encode iris features. There are two basic shapes of these filters for iris encoding, one is odd symmetric and the other is even symmetric Both the odd and even symmetric filters have zero sum in order to eliminate sensitivity

of the filter response to absolute intensity values. This is realized without effort for difference-of-sum filters, unlike Gabor filters where the even components have to be biased carefully.

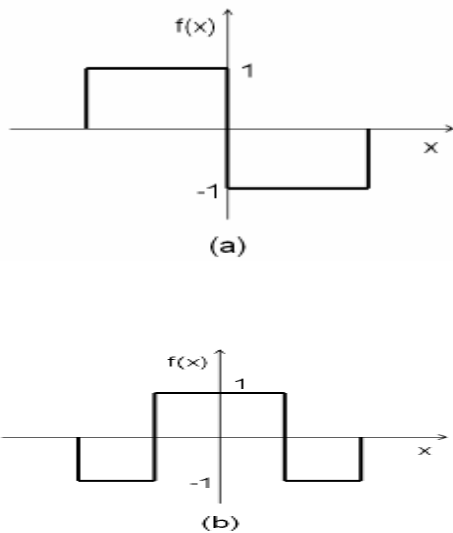


Figure4. Basic shapes of the difference of sum filters in 1D, (a) odd symmetric, and (b) even symmetric

3.5.1 Bank of Difference-of-Sum Filters

For iris feature extraction, a bank of two-dimensional difference-of-sum filters was designed and is shown in Figure5. The set of these filters have the same height but various widths. We call this special design purely horizontal scaling. We found that scaling the filters in both the horizontal and vertical directions degrades recognition performance. One possible reason is that the iris patterns may have different dependencies in the radial and angular directions [12][19]. As shown in Figure5, four pairs of odd and even symmetric filters with various widths are used for iris encoding.

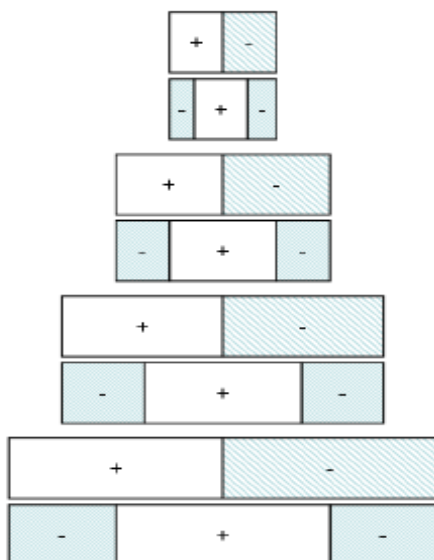


Figure5. A bank of 2D difference-of-sum filters with multiple scales in the horizontal direction. All filters have the same height.

3.5.2 Binarization

The unwrapped iris images are filtered with the set of difference-of-sum filters and the output is real valued. A sign function is then used to binarize the filtered values. The reason for the binarization is to make the encoding robust. This is important because there are quite a few sources of noise in the iris pattern. For example, the irises may be captured at different viewing angles, the incident angles of the light source(s) may change, the iris localization may be not perfect, and so on. A binarized representation with a series of “1” and “0” bits improves the robustness in iris feature encoding. The binarization is similar to digitizing an analog signal. The alteration of an analog waveform is progressive and continuous; hence it is quite sensitive to noise. While a digital signal can be quite robust. In addition to improved robustness, it also creates a very compact signature of the iris pattern.

3.5.3 Computation of Difference-of-Sum Filters

The DoS filtering can be computed rapidly with a pre-computed integral image. Crow [13][22] first proposed “summed-area tables” for fast texture mapping. Viola and Jones [14][23] used a similar idea they called the “integral image” for rapid feature extraction in face detection. Here iris feature encoding using DoS filters can also take advantage of the integral image for fast computation. The integral image at location x, y contains the sum of all the pixels above and to the left of x, y , inclusive

$$ii(x, y) = \sum_{x' \leq x, y' \leq y} I(x', y')$$

where $ii(x, y)$ is the integral image and $I(x, y)$ is the original image. Summed row by row, the

integral image can be computed quickly in one pass over the original image. Then any rectangular sum in the original image can be computed in four array

references in the integral image as shown in Figure 6.

DoS filters are different from the rectangle filters used in face detection [14][24], although both use the integral image computation. The rectangle filters [14] exhaustively search all possible scaling of the base filters for discrimination between faces and non-faces, while DoS filters are designed for the special iris patterns in a predefined manner.

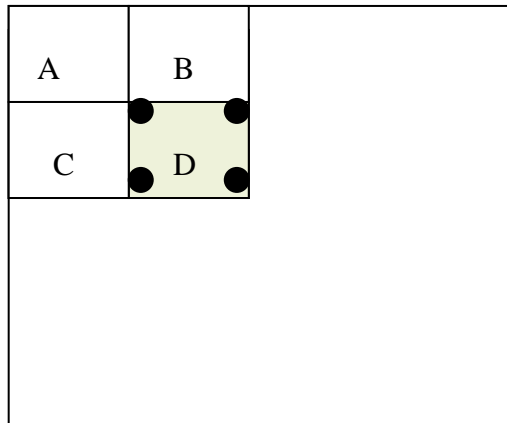


Figure 6. A rectangular sum over region D in the original image can be computed by $ii(4) + ii(1) - ii(2) - ii(3)$ in the integral image where each point contains a sum value.

3.5.4 Difference-of-Sum Filters Applied to Iris Images

To apply the set of these filters, an unwrapped iris image is divided into eight horizontal strips as shown in Figure 6. Then the filters are applied within each strip at intervals, with all these filters having the same height as each strip. Before evaluating iris recognition performance we point out some advantages of these filters over Gabor filters [4]:

1. **Simple.** There is no need to worry about any complicated implementation issues as in Gabor filter design.
2. **Fast.** Iris feature extraction with these filters is very fast. It is faster than using Gabor filters because

the only required computation in Difference-of-Sum filtering is addition or subtraction without involving multiplication or division. Thus these filters can take advantage of the integral image representation which can be computed quickly in advance.

3. **Few parameters.** all parameters such as size (width and height) and shape (odd vs. even symmetric) are explicit, without many parameters. On the other hand, Daugman's iris code uses Gabor filters with many parameters, such as the aspect ratio, wavelength, and Gaussian envelope size.

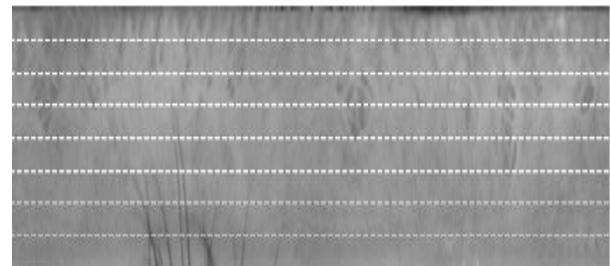


Figure 6. An unwrapped iris image is divided into eight horizontal strips before applying the Difference of Sum filters.

3.6 Experiments

To evaluate our method for iris feature encoding, we used the CASIA iris database [16] that contains 756 iris images in 108 classes. First, the irises are localized using an effective integro differential operator. The localization rate was about 84.5%. Then the detected irises are unwrapped into rectangular images and used for recognition. 200, 55 inter-class comparisons, as given in Table 1, were computed.

Table 1. Iris image database information

Database	CASIA
Number of Eyes	756
Iris Localized	647
Localization Rate	84.5%
Inter Comps	200,55

Daugman	Iris Code	Difference Of Sum	
		Filters	
Threshold	FRR FAR	FRR FAR	
0.20	0.9449 0	0.8937 0	
0.25	0.7362 0	0.6111 0	
0.30	0.3428 0	0.2393 0	
0.35	0.0608 9.6e-006	0.0262 0	
0.40	0 0.0039	0 0.0036	
0.45	0 0.5882	0 0.3344	
0.50	0 1	0 0.9848	
Decidability	4.7	5.3	

Table 2. False accept rate (FAR) and false reject rate (FRR) with respect to different separation points for difference-of-sum filters and iris code on the CASIA iris database.

2.6.1 Comparison of Difference of Sum Filters and Daugman Iris Code on the CASIA iris database.

The Difference of Sum filters are compared with Daugman's iris code [2]. The aspect ratio, wavelength, and Gaussian envelope size of the Gabor filters are unknown in Daugman's iris code [10] [11]. We tried various settings of these parameters and used the best ones in our implementation. The unwrapped iris image is of size 512×64 and divided into eight rows. The difference-of-sum filters and Gabor filters were applied to each row at the same pixel positions for sampling. The input to both methods was exactly the same in order to do a fair comparison. The heights of all the difference-of-sum filters were 8 pixels, and the widths were $12 * n$ with $n = 1, 2, 3, 4$ for the 4

pairs of odd and even symmetric filters. For the iris code method using Gabor filters, the filter bandwidth used was 3 octaves. Various wavelengths (8, 16, 24, and 32) and different aspect ratios (2 to 4) were tried and only the best settings were chosen for the four quadrature Gabor filter pairs. The number of sampling points was 256. As a result, the iris code took exactly 256 bytes for each iris image, which is the same length as in [10] [16]. These filters with binarization also resulted in a binary feature vector of 256 bytes. Computationally, difference-of-sum filtering is much faster than Gabor filtering because of its simplicity and the use of the integral image. We do not report the specific computation times here because the code for both difference-of-sum filtering and Gabor filtering are not optimized in our implementations. For iris matching, the Hamming distance [18] was computed with 6 shifts (each shift is one byte) to the left and right to compensate for iris rotation.

3.6.2 FAR and FRR

The inter-class Hamming distance distributions method is shown in Figure 7. One can see that for feature encoding deliver separated peaks for the inter-class distributions. To make a quantitative comparison, the false accept rate (FAR) and false reject rate (FRR) were computed with different separation points. As shown in Table 1, difference-of-sum filters have smaller error rates than the iris code consistently over the range of threshold values. To show the improvement of the difference-of-sum filters over the iris code method visually, the ROC curves are given in Figure 8 where the curve for these filters is much lower than that for the iris code. This suggests that difference-of-sum filtering gives smaller error rates than the iris code with various separation points. These comparisons indicate that iris features encoded by the difference-of-sum filters are more discriminative than the iris code method, and thus give higher recognition accuracy. For both methods, a good choice of the threshold value is 0.4 for intra- and inter-class separation, where both our method and the iris code have 0 FRR. Our method does have a smaller FAR of 0.0036 than the iris code FAR value of 0.0039. The threshold value of 0.4 is the same as that suggested by Masek [8] in his Matlab implementation of the iris code [16],[17].

3.6.3 Decidability

For a two-choice decision, Daugman [11] introduced the “decidability” index d to measure how well separated the two distributions are. For two distributions with means μ_1 and μ_2 , and standard deviations σ_1 and σ_2 , the decidability index d is defined as

$$d = \frac{|\mu_1 - \mu_2|}{\sqrt{(\sigma_1^2 + \sigma_2^2)/2}} \quad (3)$$

Since recognition errors are usually caused by the overlap between these two distributions, decidability measures how much the overlap is, and is independent of how the threshold is chosen to separate the two distributions. As shown in Table 2, the new features using these filters has decidability index 5.3 which is higher than the 4.7 using the Daugman iris code. This comparison also indicates that these filters have better performance for iris encoding than the Daugman iris code.

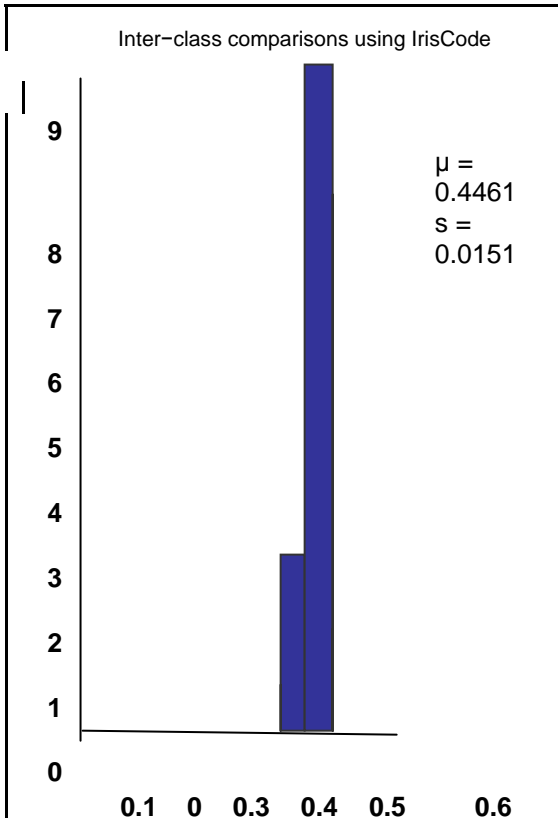
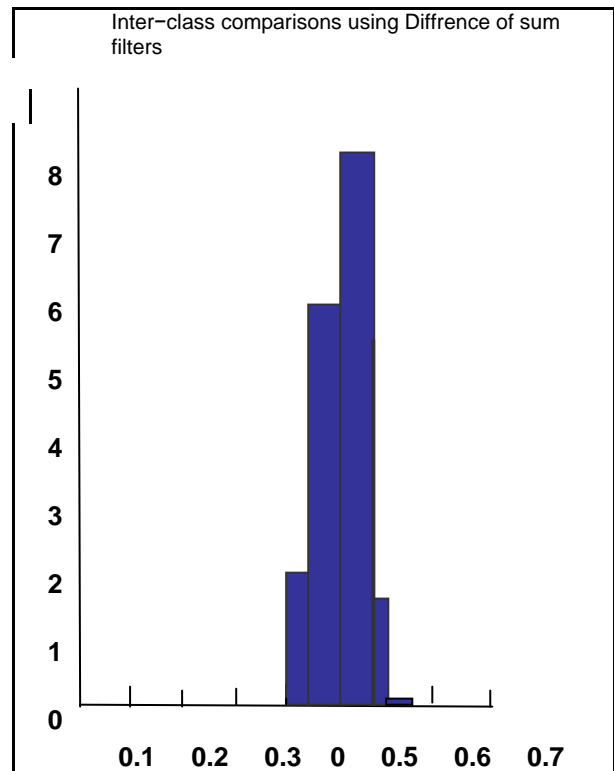


Figure 6. Interclass comparisons using Difference of Sum filters

Figure 7. Interclass Hamming distance distributions. (a) iris code and (b) difference-of-sum filters.

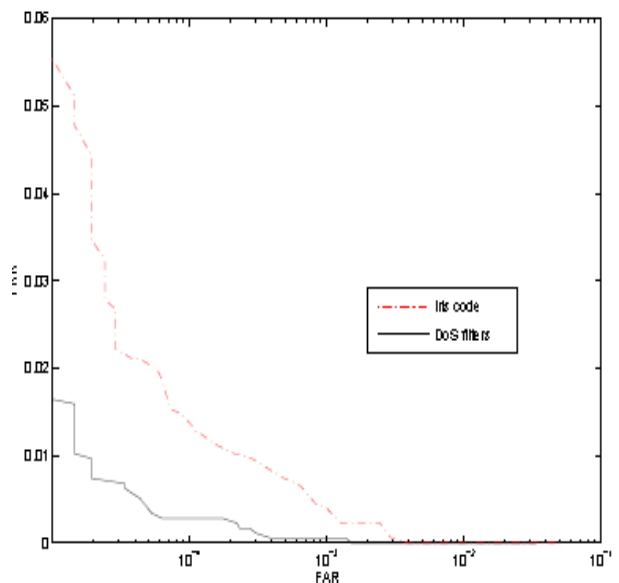


Figure 8. ROC curves showing the performance of difference-of-sum filters and iris code in terms of the FAR and FRR. These filters give smaller error

rates than the iris code method consistently at various separation points.

3.7 Conclusions

We presented a new method for iris feature encoding using difference-of-sum filters. A special design of this filter bank was proposed to characterize the iris pattern at multiple scales. One of the nice properties of these filters is that filtering can take advantage of the integral image representation, and thus all filtering takes a constant time no matter how big the filters are. Difference-of-sum filters are conceptually simple and computationally fast. Experimental results demonstrated that these filters also give higher recognition accuracy than Daugman's iris code method.

References

- [1] J. Daugman. How iris recognition works. *IEEE Trans. Circuits and Systems for Video Technology*, 14:21–30, 2004.
- [2] J. G. Daugman. High confidence visual recognition of persons by a test of statistical independence. *IEEE Trans. Pattern Analysis and Machine Intelligence*, 15:1148–1161, 1993.
- [3] Li Ma and T. Tan, "Personal Identification Based on Iris Texture Analysis," *IEEE Trans. Pattern Analysis and Machine Intelligence*, vol. 25, no. 12, 2003.
- [4] R. Wildes. Iris recognition: An emerging biometric technology. *Proc. IEEE*, 85:1348–1363, 1997.
- [5] W.W. Boles, B. Boashah: A Human Identification Technique Using Images of the Iris and Wavelet Transform. *IEEE Transaction on Signal Processing* Vol. 46 (1998) 1185-1188
- [6] S. Lim, K. Lee, O. Byeon, and T. kim. Efficient iris recognition through improvement of feature vector and classifier. *Elec. Tele. Res. Institute J.*, 23(2):61–70, 2001.
- [7] L.Ma, T. Tan, Y.Wang, and D. Zhang. Personal identification based on iris texture analysis. *IEEE Trans. Pattern Analysis and Machine Intelligence*, 25:1519–1533, 2003.
- [8] L.Masek and P. Kovesi. *MATLAB Source Code for a Biometric Identification System Based on Iris Patterns*. The School of Computer Science and Software Engineering, The University of Western Australia, 2003.
- [9] L. Ma, T. Tan, Y.Wang, and D. Zhang. Efficient iris recognition by characterizing key local variations. *IEEE Trans. Image Processing*, 13(6):739–750, 2004.
- [10] Z. Sun, T. Tan, and Y. Wang. Robust encoding of local ordinal measures: A general framework of iris recognition. In *ECCV Workshop on Biometric Authentication*, 2004.
- [11] Y. Wang and J. Han, "Iris Recognition Using Independent Component Analysis," *Int. Conf. Machine Learning and Cybernetics*, 2005, pp. 18-21.
- [12] L.Masek and P. Kovesi. *MATLAB Source Code for a Biometric Identification System Based on Iris Patterns*. The School of Computer Science and Software Engineering, The University of Western Australia, 2003.
- [13] F. Crow. Summed-area tables for texture mapping. In *Proc. SIGGRAPH 84*, volume 18, pages 207–212, 1984.
- [14] P. Viola and M. Jones. Rapid object detection using a boosted cascade of simple features. In *Proc. Computer Vision and Pattern Recognition*, volume 1, pages 511–518, 2001.
- [15] J. Daugman. How iris recognition works. *IEEE Trans. Circuits and Systems for Video Technology*, 14:21–30, 2004.
- [16] CASIA. Iris image database, 2004. <http://www.sinobiometrics.com>.
- [17] P. Viola and M. Jones. Rapid object detection using a boosted cascade of simple features. In *Proc. Computer Vision and Pattern Recognition*, volume 1, pages 511–518, 2001.
- [18] M. Negin, T. Chmielewski, M. Salganicoff, U. von Seelen, P. Venetianer, and G. Zhang. An iris biometric system for public and personal use. In *IEEE Computer*, volume 33, pages 70–75, 2000.
- [19] E. Rydgren et al. "Iris Features Extraction Using Wavelet Packet," *IEEE Int. Conf. Image Processing (ICIP)*, 2004.

[20] T. Chuan Chen, K. Liang Chung: An Efficient Randomized Algorithm for Detecting Circles. *Computer Vision and Image Understanding* Vol. 83 (2001) 172-191

[21]E. R. Davies: *Machine Vision*. 3rd Edition: Elsevier (2005).

[22] P. Kronfeld, "Gross anatomy and embryology of the eye," in *The Eye*, H. Davson, Ed. London, U.K.: Academic, 1962

[23] M. R. Chedekel, "Photophysics and photochemistry of melanin," in *Melanin: Its Role in Human Photoprotection*. Overland Park:Valdenmar, 1995, pp. 11–23.

[24] W. Boles and B. Boashash. A human identification technique using images of the iris and wavelet transform. *IEEE Trans. Signal Processing*, 46(4):1185–1188, 1998.

[25] R. P. Wildes, J. C. Asmuth, S. C. Hsu, R. J. Kolczynski, J. R. Matey, and S. E. McBride. Automated, noninvasive iris recognition system and method. U.S. Patent No. 5,572,596, 1999.